BEM Modelling of High Voltage ELF electric field applied to a 3D pregnant woman model

Cristina Peratta, Andrés Peratta,and Dragan Poljak, *Member, IEEE*

***Abstract*—The paper introduces a three dimensional multi-domain boundary element model of a pregnant woman and foetus for the analysis of exposure to high voltage extremely low frequency electric fields. The definition of the different physical and geometrical properties of the relevant tissues is established according to medical information available in existing literature. The model takes into account changes in geometry, body mass, body fat, and overall chemical composition in the body which influence the electrical properties, throughout the different gestational periods. The developed model is used to solve the case of exposure to overhead power transmission lines at different stages of pregnancy including weeks 8, 13, 26 and 38. The results obtained are in line with those published in the earlier works considering different approaches. In addition, a sensitivity analysis involving varying scenarios of conductivity, foetus postures and geometry for each stage is defined and solved. Finally, a correlation between the externally applied electric field and the current density inside the foetus is established and the zones of maximum exposure are identified.**

I. Introduction

Exposure levels in the foetus of a pregnant woman are difficult to estimate mainly because of the following. Firstly, the lack of data on electrical properties at low frequency, especially for the foetus and the surrounding tissues; secondly, the impossibility of collecting *in-vivo* measurements in a real case scenario; and finally, because of the complicated changing geometrical and physical properties of the body throughout the pregnancy period. Hence, a numerical modelling approach represents a powerful analysis tool, especially appealing for sensitivity analysis on the electrical properties which are scarce and scattered in the available literature. The aim of this work is to analyse the case of exposure of a pregnant woman to high voltage extremely low frequency (ELF) electric fields, and to apply the model to the particular case of exposure to an overhead power-line. The analysis is based on modelling the induced currents and electric fields in the foetus for different conductivity scenarios at different time stages of pregnancy, and considering different presentations of the foetus inside the maternal matrix. The differentiation in stages of pregnancies arise not only from the geometrical point of view but also from the variation of electrical properties of tissues during gestation. The amniotic fluid and foetus tissues are more conductive than the rest of the adult tissues, thus requiring a dedicated model capable of considering different shapes and conductivity scenarios.

Manuscript received and revised in February, 2010.

The material in this paper was presented in part at the 17th International Conference on Software, Telecommunications and Computer Networks (SoftCOM 2009), Split-Hvar-Korcula, Croatia, Sept. 2009.

C. Peratta and A. Peratta are with the Wessex Institute of Tehcnology, Southampton, England, UK (e-mail:{cperatta, aperatta}@wessex.ac.uk)

D. Poljak is with the University of Split, Split, Croatia (e-mail: dpoljak@fesb.hr)

II. Physical model

The model development involves two aspects, the geometrical model of the mother and foetus and the physical properties assigned to it. The conductivity of amniotic fluid changes considerably throughout gestation. Model changes including mass, volume, geometry and electrical properties of the tissues throughout gestation are considered in order to identify the the most vulnerable period.

Pregnancy is often divided into trimesters. The first 12 weeks correspond to the first trimester, weeks 13 to 28 to the second, and weeks 29 to time of birth, generally the 40^{th} week, to the third one. It is normally difficult to establish precisely the starting of the new life (fertilisation of the ovum), therefore the exact fetal age is practically impossible to determine. This is why the gestational age (measured in weeks) is more commonly used in obstetrics. Gestational age is estimated from the last menstrual period preceding fertilisation. However, in the literature, it may not always be clear which measurement criterion is applied. Fertilisation generally occurs approximately on day 14 of the menstrual cycle, or in the second week of the gestational age. In this way, the whole process of gestation is usually divided into several stages pregestation stage, which involves 2 weeks before fertilisation, pre-embryonic stage, after fertilisation, the zygote experienced a process of cell divisions ending up in the formation of the blastocyst [1]. During this period the pre-embryo is transported from the ovary through the oviduct into the uterus for implantation into the uterine wall. Implantation is completed by the end of the second week. The period from the 3^{rd} to 8^{th} week of the development is known as the embryonic period. The embryonic period is very important because this is the time when all internal and external structures develop in the embryo. In this period the different tissues and organs are developed. During this critical period, the exposure of an embryo to certain agents such as external electromagnetic fields may cause major congenital malformations.

The end of the embryonic stage occurs by the end of eighth week and then the foetal period begins. During the fetal period, the growth, development and maturation of the structures that have been already formed takes place. Henceforth, based on

TABLE I
ANTHROPOMETRIC MEASUREMENTS FOR THE FOETUS [CM]

	Week			
Measurement	**8**	**13**	**26**	**38**
CRL	4.5	10	22	35
BPD	1.8	3	6	9
AD				3.5
Leg length			13	15
Surface Area (cm^2)	27	250	850	2300

the different stages of the foetus evolution, the definition of the model reflects the four different stages of pregnancy spread along gestation. Finally, bearing these considerations in mind, the models adopted in this work correspond to the 8^{th} , 13^{th}, 26^{th} and 38^{th} gestational week.

For the maternal abdomen, the division into sub-domains is based on the different properties of the tissues. The amniotic fluid has the highest conductivity which varies depending on the period of gestation, see [2], [3] and referenced therein. Tissues such as kidney, muscle bone cortical, bladder, spleen, cartilage and skin have all conductivity values very close to 0.1 S/m, ovary and cartilage have conductivity $\sim$ 0.2 S/m. Therefore, all these tissues can be grouped into one sub-domain, namely maternal tissue. Moreover, the uterus conductivity is approximately 0.23 S/m, which is very similar to the conductivity of the maternal tissue. Hence, the uterus and maternal tissue can be included into the same sub-domain. The placenta is assumed to have the same conductivity as the blood [4]. Thus, it is considered as part of the maternal-tissue sub-domain. The maternal abdomen is divided into three sub-domains namely "maternal tissue", "amniotic fluid", contained within the uterus, and "foetus".

The geometrical definition for the foetus models was designed with the help of CT images of foetuses at different stages [5], and data on the anatomy of the mother and foe were extracted from ref. [6]. The most commonly anthropometric measurements for the size of the foetus are based on the crownrump length (CRL), and the biparietal diameter (BPD). The CRL is defined as the greatest distance between the vertex of the skull and the ischial tuberosities, with the foetus in the natural curled position [6]. The BPD is the distance between the two biparietals, and serves as a measure of the growth of the head. The BPD measurements show that growth is almost linear in the early weeks of pregnancy, but there is a progressive reduction in growth rate, especially during the final weeks. Another common fetal measurement is the abdominal diameter. Although not very common in obstetrics, the length of the leg available in the literature [1], [5] for weeks 26 and 38 was also used to define the geometry. Additionally, reference values [6] of the surface area of the foetal body were included in the definition of the geometry of the foetus. Table I summarises data on the CRL, BPD and AD throughout the different stages considered. During the foetal period, length and weight change at different rates. Foetal length change is greatest in the second trimester, while foetal weight change is greatest in the final weeks of development.

Furthermore, the foetus is free to move inside the maternal abdomen, principally until the 24^{th} week. Since then, the movement is more constrained. In obstetrics, the foetal orientation and position are normally described in terms of the *foetal lie, presentation attitude* and *position*. The *foetal lie* describes the orientation of the longitudinal axe of the foetus in relation to the longitudinal axe of the mother. If the longitudinal axe of the foetus is parallel to the longitudinal axe of the mother, the foetus is in *longitudinal lie*, while if it is perpendicular or oblique, the foetus is in *transverse* or *oblique lie* respectively. Longitudinal lie occurs in the 95% of the cases.

The fetal attitude describe the relative position of different parts of the body of the foetus in relation with his own body. For example, in the most normal fetal attitude, referred as well as *the fetal position*, the head is tucked down to the chest, with arms and legs drawn in towards the centre of the chest.

The *presentation* of the foetus refers to his orientation in relation with the birth channel. The normal presentation is cephalic presentation, with the head oriented to the birth channel. When the foetus is in cephalic presentation and fetal position, then the presentation is referred to as *vertex presentation*. This presentation is the most common at delivery and occurs in the 96% of the births. Another presentation that occurs in the 3.5% of the births is the *breech presentation* when the buttocks are oriented towards the birth channel. The last and less frequent presentation (0.5%) is the *shoulder presentation* associated with transverse lie.

In the present work, the two presentations for the different gestational ages were considered. The data for the maternal geometry and its variation along pregnancy is extracted from [6] and [2], [3]. Note that the change in volume of amniotic fluid during gestation is contemplated in the model. During the first period of gestation, the amniotic fluid is generated by the maternal plasma, but as gestation advances, foetal urine contributes to the total volume of amniotic fluid. Moreover, there is a general increase of mass distributed over the maternal body [6].

Figure 1 shows a 3D view of the model at 26 weeks of pregnancy with the foetus in cephalic presentation. All the geometrical information was introduced by means of the open source 3D preprocessor Blender [7]. This software is oriented to CAD, animation, and rendering in 3D space. To the best of the author's knowledge it has never been used before for creating meshes for BEM. Moreover the user interface and mesh generation is very appealing for BEM models of human tissues. The analysis is broken down into three parts addressing the following aspects:

- **Varying electrical conductivity.** The tissue conductivity adopted for this analysis is chosen in accordance with the data and calculations performed in [2], [8]. In [3] foetal and maternal conductivities were estimated and the values used by Dimbylow [4] summarised. The three conductivities scenarios adopted in this work are summarised in Table II, where σ_f refers to the foetus tissues conductivity, σ_{AF} to the amniotic fluid and σ_m to the maternal tissues conductivity.
- **Different time stages of pregnancy.** Four different ges-

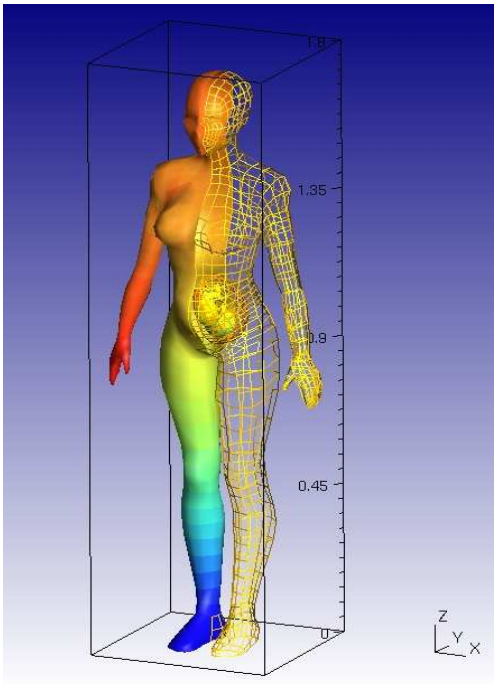

Fig. 1. Geometrical model at 26 weeks of pregnancy in cephalic presentation

TABLE II
CONDUCTIVITY SCENARIOS

		Week			
Scenario	**[S/m]**	**8**	**13**	**26**	**38**
1	σ_f	0.23	0.23	0.23	0.23
	σ_{AF}	1.28	1.28	1.27	1.10
	σ_m	0.20	0.20	0.20	0.20
2	σ_f	0.996	0.996	0.574	0.574
	σ_{AF}	1.70	1.70	1.64	1.64
	σ_m	0.52	0.52	0.52	0.52
3	σ_f	0.732	0.732	0.396	0.396
	σ_{AF}	1.70	1.70	1.64	1.64
	σ_m	0.17	0.17	0.17	0.17

tational ages are considered in this work corresponding to 8, 13, 26 and 38 weeks.

- **Different presentations of the foetus.** Two different presentations have been considered for each gestational age.

III. BEM FOR VERTICALLY INCIDENT FIELD IN OPEN ENVIRONMENTS

The numerical approach is based on the direct boundary element method with the collocation technique [9]. The main advantages of the method are first that volume discretisation of the geometry is avoided, thus allowing to solve complicated geometries, second that the formulation is based on the exact solution of the leading partial differential operator rather than on approximating functions, thus allowing high accuracy; and third that separate degrees of freedom are used for the

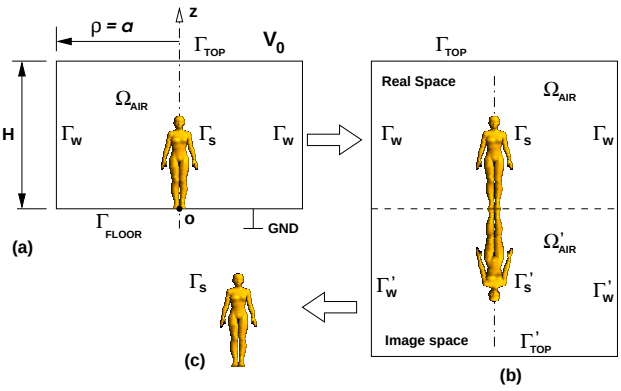

Fig. 2. Simplification of the conceptual model. (a) Original conceptual model. (b) Floor disretisation is avoided by reflecting the problem. (c) Top and lateral wall discretisation is replaced with asymptotic analytical integrations.

main unknown (potential) and its gradient or derived flux in normal direction to the boundaries (normal current density). In other words, normal current densities are not computed by numerical differentiation of the obtained potential, but they are produced as a direct outcome of the method. The BEM implemented in this work contemplates constant, linear and quadratic elements of triangular and quadrilateral geometry. However, a good balance between accuracy and computational burden was obtained with a mixture between constant and linear elements. Therefore quadratic elements were avoided.

In general, one of the major drawbacks of the method when applied in its traditional form, is that it leads to a fully populated linear system of equations, which is hard to solve with standard methods based on direct Gauss elimination for large number of degrees of freedom. However, this can be overcome with preconditioning techniques such as fast multipole methods or adaptive cross approximations [10]. The conceptual model for the model to solve is shown in Fig. 2-(a). The integration domain consists of the human body and the volume of air enclosed within the floor, ceiling and lateral walls represented by surfaces Γ_{FLOOR} at $z = 0$, Γ_{TOP} at $z = H$, and Γ_{W} at $\rho = a$, respectively, in a cylindrical system of coordinates with origin o. The top surface Γ_{TOP} is considered as an imaginary flat equipotential surface with constant voltage given by $\varphi(z = H) = V_0$, while the floor is at potential $\varphi(z = 0) = 0$.

In an open environment, the lateral walls Γ_w are assumed to be far from the body (i.e. $\rho = a \to \infty$) with potential given by: $\varphi|_{\text{wall}} = zV_0/H$, and normal electric field $E_n = 0$. Because of the symmetry of the problem, it is possible to eliminate the discretisation of all the external boundaries by means of the following assumptions. The floor, considered as a perfectly conductive plane, can be eliminated by introducing an image space, as shown in Fig. 2-b. The potentials and electric fields in the imaginary space are the same as the ones in the real space but with opposite sign. Hence: $\varphi(x, y, z) = -\varphi(x, y, -z)$ and $E_n(x, y, z) = E_n(x, y, -z)$. In this way, the discretisation of the floor is no longer required and several hundred elements can be spared. In the next step, the discretisation of the lateral and top surfaces, as well as their corresponding images are also removed by analytical integration, thus saving more degrees

of freedom. Finally, the discretisation for the external problem , i.e. involving the air and the human body, consists only of surface elements on the skin of the body. In this way, the level of discretisation is reduced and conveniently simplified leading to two main advantages: firstly a reduction in the number of degrees of freedom of typically few thousand elements with respect to a standard model in which the body is inside a box; and secondly, rather more technical, the model construction for changing shapes of human body becomes simpler, since the shape of the "air", regarded as a sub-domain surrounding the body, does not need to be re-defined each time the skin changes its shape.

The rest of this section explains how the discretisation on lateral and top walls in both real and imaginary space can be eliminated by means of analytical integrations.

The relevant integral equation for the potential φ at $\mathbf{x}_s \in \Omega_{\text{air}}$ is given by:

$$c(\mathbf{x}_s)\varphi(\mathbf{x}_s) + \int_{\Gamma} \frac{\partial G(\mathbf{x},\mathbf{x}_s)}{\partial n}\varphi(\mathbf{x})d\Gamma - \int_{\Gamma} G(\mathbf{x},\mathbf{x}_s)E_n(\mathbf{x})d\Gamma = 0, \quad (1)$$

where G is the Green's function of Laplace equation, i.e.: $\nabla^2 G(\mathbf{x},\mathbf{x}_s) + \delta(\mathbf{x},\mathbf{x}_s) = 0$, $\Gamma = \partial(\Omega)$ is the boundary of the air surrounding the body, composed of the lateral walls Γ_w, the top surface Γ_{TOP} and the skin Γ_s including the real and imaginary space; i.e. $\Gamma = \Gamma_w \cup \Gamma_{\text{TOP}} \cup \Gamma_s \Gamma'_w \cup \Gamma'_{\text{TOP}} \cup \Gamma'_s$. The goal is to take advantage of the symmetry and asymptotic behaviour of the solution of the problem in order to eliminate the mesh discretisation in Γ_{W}, Γ_{TOP} and Γ_{FLOOR}.

A. Analytical approach for lateral walls and top surface

The integration for the double and single layer potentials in Γ_{W} can be done in cylindrical coordinates as follows:

$$I^1_w = \int_{\Gamma_{\text{W}}} \frac{\partial G(\mathbf{x},\mathbf{x}_s)}{\partial n}\varphi(\mathbf{x})d\Gamma = \int_{\theta=0}^{2\pi}\int_{z=0}^{H} \frac{-1}{4\pi\rho^2}\frac{zV_0}{H}\rho d\theta dz = -\frac{V_0 H}{4\rho} \quad (2)$$

Therefore, the above integral tends to zero when $\rho \to \infty$. In addition, the single layer potential integral becomes zero, since $E_n = 0$, i.e.: $\int_{\Gamma_W} GE_n \, d\Gamma = 0$. At the top surface the normal derivative of G becomes:

$$\frac{\partial G}{\partial n} = -\frac{\mathbf{r}\cdot\hat{n}}{4\pi r^3} = -\frac{H - z_s}{4\pi\left(\rho^2 + (H-z)^2\right)^{3/2}} \quad (3)$$

where $r = \|\mathbf{x} - \mathbf{x}_s\|$. The potential is fixed: $\varphi = V_0$, and $d\Gamma = \rho \; d\rho \; d\theta$. Therefore the integral of the double layer potential is written as:

$$I^1_T = \int_{\Gamma_{\text{TOP}}} \frac{\partial G}{\partial n}\varphi d\Gamma = \int_{\theta=0}^{2\pi}\int_{\rho=0}^{a} \frac{(z_s - H)\,V_0\rho \; d\rho \; d\theta}{4\pi\left(\rho^2 + (H-z)^2\right)^{3/2}}, \quad (4)$$

which results into:

$$I^1_T = \frac{(z_s - H)\,V_0}{2}\left\{\frac{-1}{\sqrt{a^2 + (H-z)^2}} + \frac{1}{|H-z|}\right\}. \quad (5)$$

then, in the limit $a \to \infty$, expression (5) becomes: $\lim_{a\to\infty} \int_{\Gamma_{\text{TOP}}} \frac{\partial G}{\partial n}\varphi d\Gamma = -\frac{V_0}{2}$. By repeating these steps in the imaginary surface Γ'_{TOP}, the following result is obtained: $\lim_{a\to\infty} \int_{\Gamma'_{\text{TOP}}} \frac{\partial G}{\partial n}\varphi d\Gamma = \frac{V_0}{2}$. Finally, these last two double layer potential integrals cancel with each other, yielding:

$$\lim_{a\to\infty}\left\{\int_{\Gamma_{\text{TOP}}} \frac{\partial G}{\partial n}\varphi \; d\Gamma + \int_{\Gamma'_{\text{TOP}}} \frac{\partial G}{\partial n}\varphi \; d\Gamma'\right\} = 0. \quad (6)$$

The integral of the single layer potential due to sources in the top surface of the real space is written as follows: $I_{\text{TOP}} = \int G(\mathbf{x},\mathbf{x}_s)E_n \; d\Gamma$, where $G(\mathbf{x},\mathbf{x}_s) = (4\pi r)^{-1}$, $r = \sqrt{\rho^2 + (H-z)^2}$, $d\Gamma = \rho \; d\theta \; d\rho$, and $E_n = \nabla\varphi\cdot\hat{n} = \frac{V_0}{H}$. Therefore, I_{TOP} becomes:

$$I_{\text{TOP}} = \int_{\theta=0}^{2\pi}\int_{\rho=0}^{a} \frac{V_0\rho d\rho \; d\theta}{4\pi H\sqrt{\rho^2 + (H-z)^2}} = = \frac{V_0}{2H}\left[\sqrt{a^2 + (H-z)^2} - (H-z)\right]. \quad (7)$$

Analogously for the imaginary space, it results:

$$I'_{\text{TOP}} = \int_{\theta=0}^{2\pi}\int_{\rho=0}^{a} \frac{-V_0\rho d\rho \; d\theta}{4\pi H\sqrt{\rho^2 + (H+z)^2}} = -\frac{V_0}{2H}\left[\sqrt{a^2 + (H+z)^2} - (H+z)\right]. \quad (8)$$

In the limit when $a \to \infty$ the total integral given by $I_{\text{TOP}} + I'_{\text{TOP}}$ from (7) and (8) becomes: $\lim_{a\to\infty}[I_{\text{TOP}} + I'_{\text{TOP}}] = \frac{zV_0}{H}$. Finally, when $a \to \infty$, the integral equation (1) for the air sub-domain, can be replaced by: $-\frac{zV_0}{H}$, which involves only two integrals in the skin surface of the body, one for the single layer potential and another for the double layer potential.

IV. Numerical implementation

The conceptual model consists of a homogeneous anatomical shape of pregnant woman (body) with the uterus and foetus immersed in it. The body is placed in an open environment, standing barefoot on a perfectly conductive infinite flat surface at $z = 0$, at ground level ($\varphi = 0$.) This represents the worst case scenario for open environments in which currents throughout the body are expected to be maximum.

The pregnant woman is exposed to a reference field oriented in z direction, with asymptotic value $E_0\hat{\mathbf{z}}$ when $z \to \infty$, as shown in Figure 2. These conditions are recreated by fixing an equi-potential plane $\varphi = V_0$ at $z = H$, where H is sufficiently larger than the height of the woman, and then scaling up the results by a factor $\theta = H/V_0 \times E_0$, in order to translate the results into a particular magnitude of incident field E_0. In particular, the results obtained in this work were obtained by

adopting $V_0 = 1V$ and $H = 5m$. Then, for example, in order to translate the results to the case of $E_0 = 10kV/m$, a factor $\theta = 5 \times 10^7$ which multiplies $\mathbf{j}$ is adopted in order to obtain $\mathbf{j}$ in mA/m^2.

The BEM model of consists of four sub-domains, Ω_{AIR}, Ω_{BODY}, Ω_{AF} and Ω_{F}, namely air, body, amniotic fluid and foetus, respectively. The air is bounded by Γ_{TOP}, Γ_{W}, Γ_{FLOOR} and Γ_S; while the body is bounded by Γ_{s} and $\Gamma_{ti},\ i = 1, \cdots, N_t$, where Γ_{ti} represents the surface enclosing the different internal organs embedded in the homogeneous body, and N_t is the number of organs. Part of Γ_S is in contact to the ground Γ_{SF}, while the rest is in contact to the air Γ_{SA}.

Table III summarises the relationship between sub-domains, surfaces and boundary conditions in the model.

TABLE III
SOLVING STRATEGY. CONNECTIVITY BETWEEN SUB-DOMAINS AND SURFACES INVOLVED IN THE MODEL OF PREGNANT WOMAN, AND BOUNDARY CONDITIONS APPLIED TO EACH SURFACE. "×" SYMBOL INDICATES AN UNKNOWN OF THE PROBLEM.

COUPLED MODEL								
	Ω_{AIR}		Ω_{BODY}		Ω_{AF}		Ω_{F}	
	φ	E_n	φ	E_n	φ	E_n	φ	E_n
Γ_{TOP}	V_0	×	-	-	-	-	-	-
Γ_{W}	$\frac{zV_0}{H}$	0	-	-	-	-	-	-
Γ_{FLOOR}	0	×	-	-	-	-	-	-
Γ_{SA}	×	×	×	×	-	-	-	-
Γ_{SF}	-	-	0	×	-	-	-	-
Γ_{T1}	-	-	×	×	×	×	-	-
Γ_{T2}	-	-	-	-	×	×	×	×

=

STAGE 1			
Ω_{AIR}		Ω_{BODY}	
φ	E_n	φ	E_n
V_0	$\frac{V_0}{H}$	-	-
$\frac{zV_0}{H}$	0	-	-
0	×	-	-
×	×	×	×
-	-	0	×
-	-	-	-
-	-	-	-

+

STAGE 2					
Ω_{BODY}		Ω_{AF}		Ω_{F}	
φ	E_n	φ	E_n	φ	E_n
-	-	-	-	-	-
-	-	-	-	-	-
-	-	-	-	-	-
φ_s	E_{ns}	-	-	-	-
0	×	-	-	-	-
×	×	×	×	-	-
-	-	×	×	×	×

The "×" symbol in the table indicates an unknown, while "-" symbol indicates that the corresponding surface is not related to the sub-domain.

The complete problem involves the air (considered as an external problem), and the body with its internal organs and the foetus. In order to reduce as much as possible the computational burden, the solution approach with BEM is split into two parts, corresponding to the internal and external problem. Hence, the BEM solving approach consists of two stages: 1 and 2.

Stage 1 solves the external problem, involving the air coupled to the homogeneous body (i.e. without internal tissues). The aim of stage 1 is to find the electric field and potential in the skin, considering it as an interface separating air from body. Note that the inclusion of the body without internal tissues does not introduce significant errors in the results on the skin, as proved in [2].

The values of potential and normal electric field obtained for the skin from the second stage are imposed as boundary conditions in order to solve the interior problem in the second stage. The interior problem consists of the body, amniotic fluid and foetus. The outcomes of the second stage are potentials and normal fluxes at the interfaces of the internal tissues, i.e. Γ_{T1} and Γ_{T2}. Finally, these fields are used to compute the solution for $\mathbf{j}$, $\mathbf{E}$ and φ at internal observation points.

V. RESULTS AND DISCUSSION

Figure 3 shows a lateral view of the sliced model of the pregnant woman. The direction of the electric field in the maternal tissues is shown by black arrows. The iso-lines represent the electric potential field. The naming convention assigned to the different models is composed by letter "B" followed by two digits indicating the pregnancy week (08,13,26, or 38), followed by a single digit (1,2,or 3)indicating the conductivity scenario established in Table II and a letter "U" or "D" for cephalic or breech position, respectively.

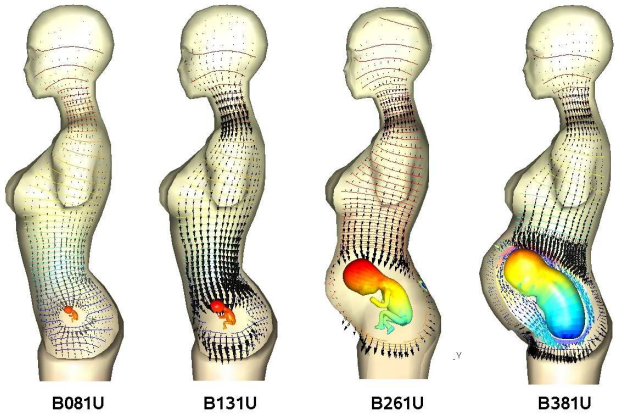

Fig. 3. Lateral view

A. Current density along the foetus

Figure 4 shows the observation line that goes along the spine of the foetus, where the current density has been measured. Figure 5 shows $|\mathbf{J}|$ in function of z along the observation line $\bar{AB}$ inside the foetus. The incident field has been scaled to 10 kV/m and the currents are expressed in mA/m^2. The figure illustrates the numerical findings at different weeks of pregnancy in the three different conductivity scenarios. Each plot compares the same results for the cephalic and breech

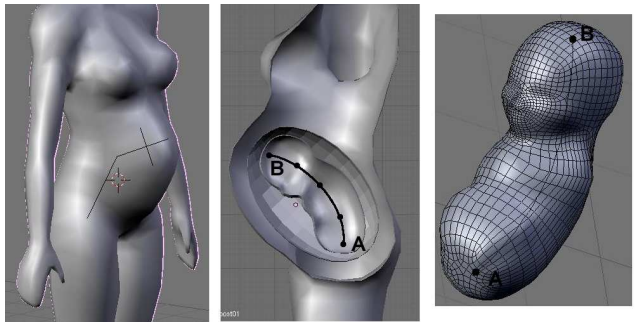

Fig. 4. Observation line along the spine of the foetus

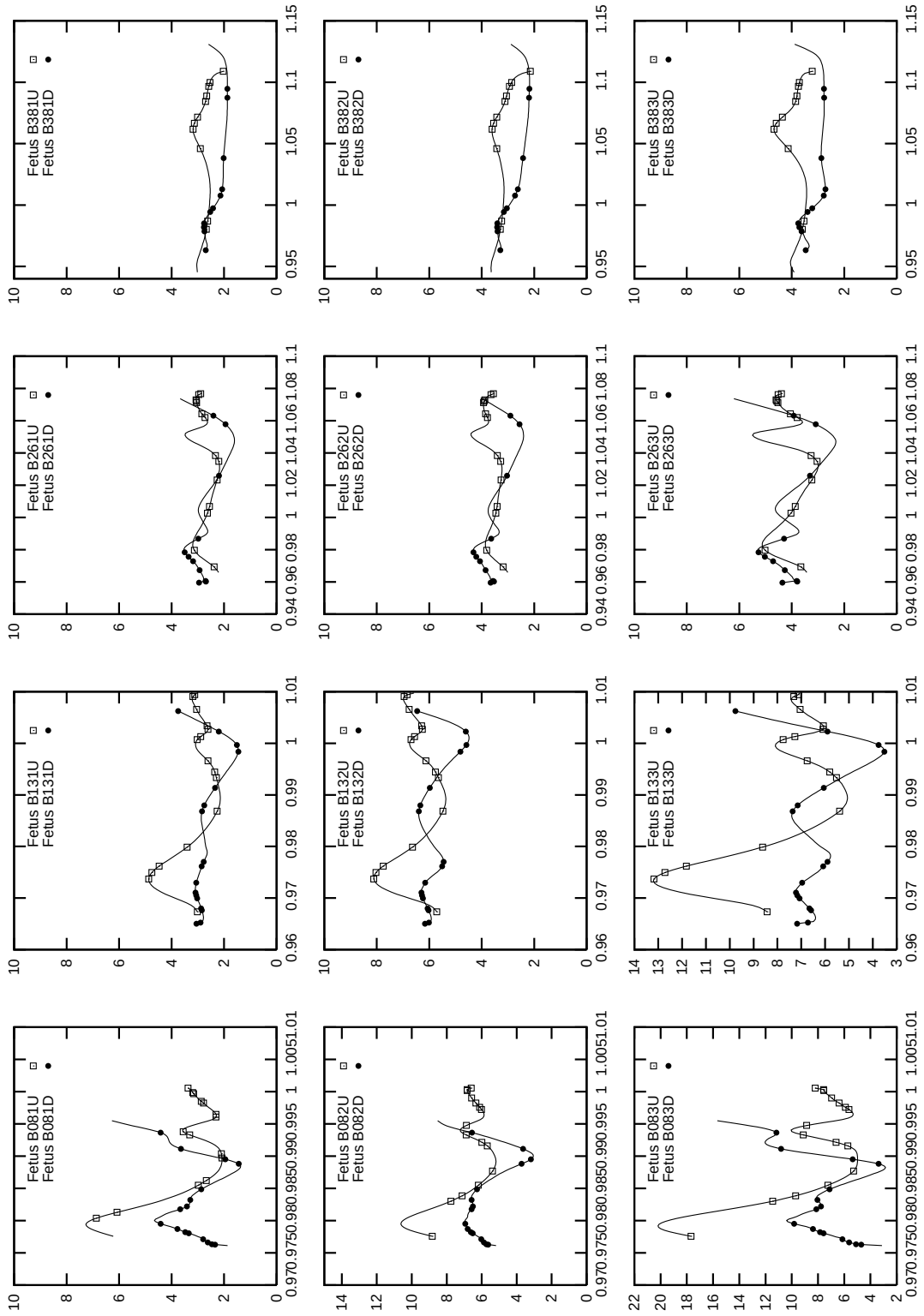

Fig. 5. Current density along the spine of the foetus. Scenarios 1,2 and 3. Ages: 8,13,16 and 38 weeks

presentations.

Each row in Figure 5 corresponds to a particular conductivity scenario (i.e. first row corresponds to scenario 1, and so on), while each column corresponds to a particular gestational age (i.e. first column represents 8^{th} week, second to 13^{th} week, third to 26^{th} and forth to 38^{th}).

1) Current Density variation throughout gestation: As shown along a row in Figure 5 the maximum values of current density are obtained at the 8^{th} gestational week, then it decreases progressively as the foetus develops. This behaviour

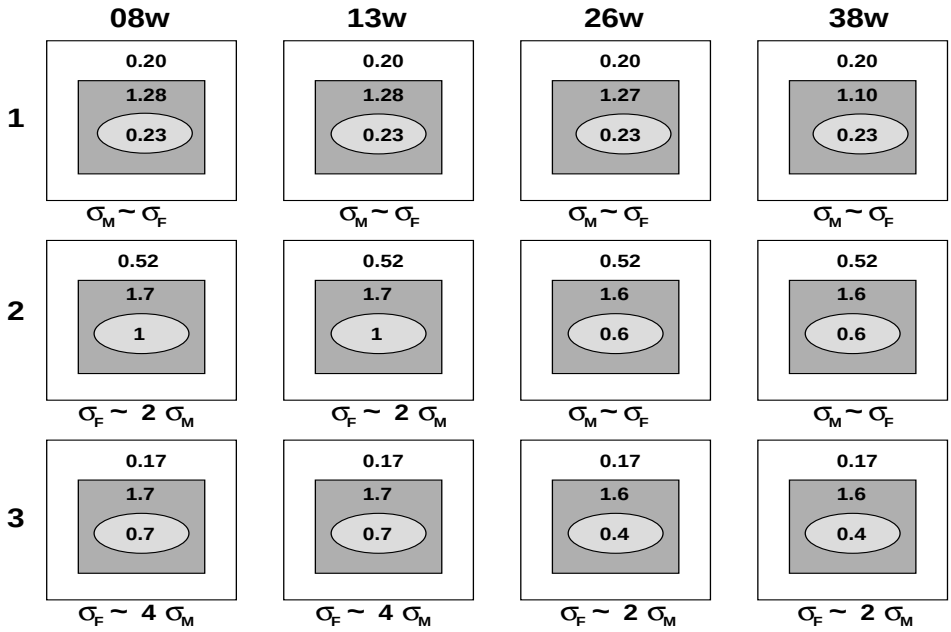

Fig. 6. Scenarios illustration showing the relation between maternal and foetus conductivities

is observed in the three conductivity scenarios. The decrease of current density flowing through the foetus with age, can be explained as a consequence of the two following factors. First, the foetus conductivity as well as the amniotic fluid conductivity decrease with age. Second, as the foetus grows, he tends to adopt a *vertex presentation* (extremities drawn in towards the centre of the chest and head tucked down to the chest), hence his external surface becomes smoother and the cross sectional area becomes more regular.

2) Differences in current density between conductivity scenarios: Figure 6 shows the relation between foetal and maternal tissue conductivity for each scenario and gestational age arranged in the same order as in figure 5. The current flows preferentially through pathways of high conductivity. The amniotic fluid conductivity is more or less high and constant in different scenarios and gestational ages. Therefore, the relation between maternal and foetal tissues conductivities will contribute to determine the pathways of current. Figure 5, shows that for all gestational ages the current density in the foetus in the case of scenario 3 is bigger than in scenario 2, and in scenario 2 is bigger than scenario 1. However, the high contrast in current densities observed between scenarios in weeks 8 and 13, is attenuated in weeks 26 and 38. This behaviour can be explained by considering the ratios between foetal and maternal conductivities shown in Figure 6. In the case of scenario 1, foetal conductivity is similar to maternal tissues conductivity, while for scenarios 2 and 3 foetal conductivity is bigger. Therefore, the current density in scenario 3 is expected to be bigger than in scenario 2, and the latter bigger than in scenario 1. However, in scenario 2 (and 3), weeks 8 and 13, the foetus conductivity is approximately 2 (and 4) times bigger than the maternal tissue conductivity respectively. On the other hand, for weeks 26 and 38, the foetus conductivity is approximately similar (and 2 times bigger) than the maternal conductivity. Thus, the contrast in current densities between scenarios becomes attenuated in week 26 and 38.

3) Current Density variation with the presentation of the foetus: The comparison of current densities induced in the foetus between the two different presentations considered (breech and cephalic), shows that for all scenarios and gestational ages the breech presentation gives higher current densities along the body of the foetus. This effect is less pronounced in the last stage of pregnancy (38 week), which can be explained by considering that the part of the body with bigger cross sectional area (i.e. the head) is exposed to a higher field when the foetus is in breech presentation, thus giving rise to higher currents flowing along the body. As the foetus grows, he tends to adopt the *foetal position* attitude, and his cross sectional becomes more regular, thus decreasing the difference in current density between the two presentations.

B. Mean and Extreme Values of Current Density in the foetus

Figures 7 show the mean, maximum and minimum values of current density computed in the foetus at different weeks of pregnancy. The results compile the maximum and minimum values of current density ($j = \sigma_f |\nabla \varphi|$) calculated along the spine of the foetus, including the two different presentations: cephalic and breech. The trend observed in the results is that the current density inside the foetus decreases with age. This is due to the increasing uniformity of the foetus model, where the geometry is smoother and less fluctuations are expected in the results. According to the results shown in Figures 7, the maximum value of current density in the foetus occurs during the 8^{th} week for all considered conductivity scenarios. For an incident external field of 10 kV/m the current density in the foetus is approximately 7.5 mA/m^2. The maximum value recommended for public exposure by ICNRP [11] is 2 mA/m^2, which is achieved in the foetus when an external electric field $E_1 \approx 3$ kV/m is applied. Another region presenting high current density under vertical incidence of electric field is in

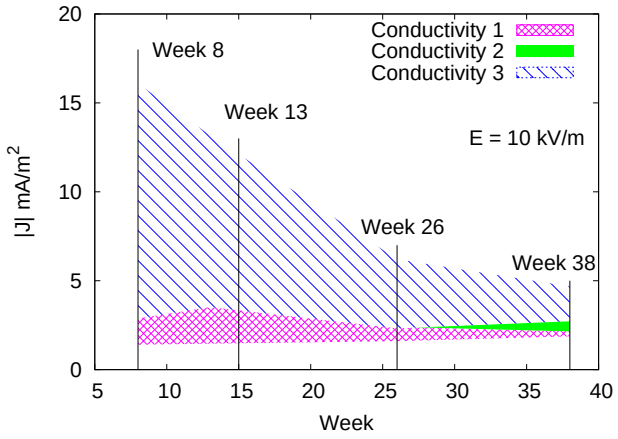

Fig. 7. Mean current density in the foetus during gestational period for all conductivity scenarios

the mother's brain and neck. $|J_{max}|$ in the brain decreases from $\approx$ 0.43 to $\approx$ 0.41 mA/m^2 from week 8 to week 38. As expected, this value is not sensitive to the different conductivity scenarios related to pregnancy.

VI. Conclusions

A 3D multi-domain boundary element model of a pregnant woman and foetus at four different stages of pregnancy has been developed and used to analyse different cases of exposure to high voltage extremely low frequency electric field. The definition of the different physical and geometrical properties of the most influential tissues from the foetus point of view has been established following the medical information available in the literature. The case of exposure to overhead power transmission lines was solved and analysed. The results obtained for the different stages of pregnancy are in good agreement with those published in the existing literature. A test matrix of different scenarios involving three sets of conductivity, two foetus postures and four pregnancy stages has been defined and solved. The results allowed obtaining mean values as well as maximum and minimum deviations of induced currents and electric fields in the foetus.

In general, the contrast of conductivity between foetus, amniotic fluid and maternal tissue is a key factor for the maximum induced currents in the foetus. Moreover, the maximum current density appearing in the foetus changes throughout the gestational period mostly due to geometrical changes, posture and electrical properties of the surrounding tissues.

References

[1] M. F. MJT and M. FitGerald, *Human Embryology*. London: W. B Sauders Company, 1994.

[2] C. González, "Electromagnetic exposure to elf electric fields using parametric models of the human body and bem," Ph.D. dissertation, University of Wales, 2008.

[3] C.Peratta and A. Peratta, *Modelling the Human Body Exposure to ELF Electric Fields*. WIT Press, 2010.

[4] P. Dimbylow, "Development of pregnant female, hybrid voxel mathematical models and their application to the dosimetry of applied magnetic and electric fields at 50 hz," *Phys. Med. Biol.*, vol. 51, pp. 2383–94, 2006.

[5] "UNSW Embriology - Dr.Mark Hill," Website, University of New South Wales, Sidney, Australia. [Online]. Available: http://embryology.med.unsw.edu.au/embryo.htm

[6] I. 2002, "Basic anatomical and physiological data for use in radiological protection: reference values," *ISNN 0146-6453*, vol. 89, 2002.

[7] "Blender," Website. [Online]. Available: www.blender.org

[8] C. Gonzalez, A. Peratta, and D. Poljak, "Electromagnetic modelling of foetus and pregnant woman exposed to extremely low frequency electromagnetic fields," in *Boundary Elements and Other Mesh Reduction Methods XXX*, 1st ed., ser. Transactions on Modelling and Simulation, L. Skerget, Ed. WIT Press, 2008, vol. 47, book Advanced Computational Techniques, pp. 85–94.

[9] C. Brebbia and J.Dominguez, *Boundary Elements, an Introductory Course*, 2nd ed., ser. Computational Mechanics Publications. New York, Colorado, San Francisco, Mexico, Toronto: McGraw-Hill, 1992.

[10] T. Grytsenko and A. Peratta, "Adaptive cross approximation based solver for boundary element method with single domain in 3D," in *Boundary Elements and Other Mesh Reduction Methods XXX*, 1st ed., ser. Transactions on Modelling and Simulation, L. Skerget, Ed. WIT Press, 2008, vol. 47, book Advanced Computational Techniques, pp. 209–218.

[11] ICNIRP, "Guidelines for limiting exposure to time-varying electric, magnetic, and electromagnetic fields (up to 300 ghz)," *Health Physics.*, vol. 74, no. 4, pp. 494–522, 1998.

Cristina Peratta received her MSc in Physics in 1996 from University of Buenos Aires (Faculty of Exact and Natural Sciences), Argentina, and her PhD in 2008 from University of Wales, UK. Her background is in Numerical Modelling applied to Electromagnetic problems. She developed her graduate thesis at the Plasma Physics Institute, (INFIP), University of Buenos Aires-CONICET, Argentina, in numerical modelling applied to Nuclear Fusion in Z-pinch experiments. Her PhD thesis was oriented to numerical modelling applied to human exposure to electromagnetic fields in the extremely low frequency range.

Andrés Peratta received his MSc in Physics in 2001 from University of Buenos Aires, Argentina, and his PhD in 2004 from University of Wales, UK. During 2005 he has been a Postdoctoral Fellow and Assistant Professor at the Wessex Institute of Technology (WIT), Southampton UK and became member of the Editorial Board of Journal of Communications, Software and Systems (JCOMSS) sponsored by IEEE and SoftCom Society. In 2006 he became Head of the ICE Division at Wessex Institute of Technology and ISAC member of the WIT International Conferences on Environmental Electromagnetic Compatibility, Simulation of Electrochemical Processes, and Computational Ballistics. His research interests are Numerical Modelling, Boundary and Finite Element methods, Electromagnetism, Computational Fluid Dynamics and Continuum Mechanics.

Dragan Poljak received his BSc in 1990, his MSc in 1994 and PhD in 1996 from the University of Split, Croatia. He is the Full Professor at the Department of Electronics at the University of Split, and he is also Adjunct Professor at Wessex Institute of Technology, UK. His research interests include frequency and time domain computational methods in electromagnetics, particularly in the numerical modeling of wire antenna structures, and recently numerical modeling applied to environmental aspects of electromagnetic fields. To date Professor Poljak has published more than 180 journal and conference papers in the area of computational electromagnetics, four authored books and one edited book, by WIT Press, Southampton-Boston. Professor Poljak is a member of IEEE, a member of the Editorial Board of the journal Engineering Analysis with Boundary Elements, and co-chairman of the WIT International Conference on Computational Methods in Electrical Engineering and Electromagnetics, and International Conference on Environmental Electromagnetics. He is also editor of the WIT Press Series Advances in Electrical Engineering and Electromagnetics. Recently, professor Poljak was awarded by the National Prize for Science.